Reinforcement Effect and Molecular Motions in Semicrystalline PEEK Films: Mechanical and Physical Modelings. I

C. BAS, M. FUGIER, N. D. ALBÉROLA

Laboratoire Matériaux Polymères et Composites, Université de Savoie, Campus Scientifique, Bâtiment IUT, F-73376 Le Bourget-du-Lac Cedex, France

Received 19 June 1996; accepted 18 September 1996

ABSTRACT: The influence of the crystalline phase on the viscoelastic behavior of poly (aryl ether ether ketone) (PEEK) films is assessed by dynamic mechanical spectrometry. Prediction of the viscoelastic behavior near T_g of semicrystalline films is performed through mechanical and physical modelings. Changes in the α relaxation induced by the crystalline phase are related to both the mechanical coupling between phases and the decrease in the molecular mobility of chains, which is improved for samples showing a broad crystallite size distribution. Crystalline phase also induces some modifications in the characteristics of the β spectrum. The reinforcement effect brought by the crystalline phase in such a temperature range is predicted through a mechanical model. Then, changes in tan δ level in the β_1 region induced by the crystalline phase result from the mechanical coupling between phases. The magnitude of such changes only depends on the crystallinity ratio and it is not controlled by the crystallite size distribution. The crystalline phase also induces changes in the pattern of the β_2 transition, which could be attributed to modifications in the conformations of the chains near the crystalline entities and/or the magnitude of interactions between chains. Such modifications seem to be sensitive to the thermal history of PEEK samples. © 1997 John Wiley & Sons, Inc. J Appl Polym Sci **64:** 1041–1052, 1997

Key words: Poly(aryl ether ether ketone); viscoelastic behavior; mechanical coupling; molecular mobility; semicrystalline polymer

INTRODUCTION

Microstructure of semicrystalline poly(aryl ether ether ketone) (PEEK) has been extensively studied by using various methods such as differential scanning calorimetry (DSC), infrared spectroscopy, wide angle X-ray diffraction (WAXS), and electron microscopy.[1–17] It was shown that the microstructure displayed by semicrystalline PEEK specimen is complex and strongly depends on the thermal history undergone by samples. Thus, there is a large controversy about the melting behavior of PEEK. As a matter of fact, according to the crystallization conditions, semicrystalline PEEK could exhibit one or more melting peaks.[1,13–17] In a previous work,[17] we have related the double melting behavior to a bimodal distribution in size and/or perfection degree of crystalline entities developed in a two-step crystallization.

Microstructure of PEEK can be also assessed in terms of molecular motions. Thus, it was shown that the crystalline phase induces changes in the characteristics of the main relaxation related to T_g of the polymer.[18–21] From a qualitative point of view, such changes were interpreted in terms of modifications of the molecular mobility involving large segments of the macromolecular chains in

Correspondence to: N. D. Albérola.
 CCC 0021-8995/97/061041-12

the amorphous phase; but conclusions from dynamic mechanical spectrometry investigations completely neglect the influence of the mechanical coupling between phases, i.e., the reinforcement effect brought by crystalline entities, which could lead to similar modifications of the main mechanical relaxation as those induced by interactions between phases. Moreover, the influence of the thermal treatment conditions, i.e., the broadness of the crystallite size distribution, on the dynamic mechanical behavior of semicrystalline PEEK was not finely analyzed.

Furthermore, there are few reports in the literature concerning the influence of the crystalline phase on the β spectrum.[18,19,22–24] All works conclude to a decrease in the magnitude of the β spectrum due to interactions between phases, but such a physical interpretation also neglects the contribution of the mechanical coupling between phases on the micromechanical behavior in such a temperature range.

The aim of this work is to quantify the respective contributions of the mechanical coupling effect and the influence of the interactions between phases in semicrystalline PEEK films on the β and α mechanical relaxations. Thus, dynamic mechanical behaviors of PEEK films showing different thermal histories are investigated in the α and β regions. A mechanical model is used to quantify the influence of the reinforcement effect of the amorphous phase by crystalline entities. Then, after separating the mechanical behavior of the two phases through such an approach, the magnitude of interactions between the amorphous and the crystalline phases is evaluated through a physical modeling applied in the T_g region. Characteristics of the crystalline phase, i.e., crystallinity ratio, size distribution, and perfection degree of crystalline entities are investigated by DSC, WAXS, and density measurements.

EXPERIMENTAL

Materials

Sheets of amorphous PEEK films with thickness of 100 and 250 μm were provided by ICI Company. Figure 1 shows the WAXS profile of an as-received film. The average molecular weight and polydispersity index determined by the Laboratoire des Hauts Polymères (Université Catholique de Louvain-la-Neuve, Belgium)[25] are $\overline{M_w}$ = 38,000 g/mol and I_p = 2.2, respectively.

Before any analysis, as-received films were dried at 145°C for six hours under vacuum. Then, to erase the previous thermal history and to give the same isoconfigurational state at each sample, specimens were heated for 10 min at a temperature higher than the glass transition and then quenched at room temperature. Such films are then controlled by WAXS to ensure that no crystallization has occurred during these thermal treatments.

Semicrystalline PEEK films were obtained by annealing as-received films for 30 min at different temperatures (Table I). The as-received amorphous film is designed as Q, and the annealed samples as A, followed by the annealing temperature (Table II).

Wide-angle X-ray Scattering

The wide-angle X-ray diffractograms of the as-received and annealed samples were recorded at room temperature by using a INEL CPS 120 diffractometer (Co $K_{\alpha 1}$ filtered radiation) with 0.02 degree (2θ) scan increments. The crystalline structure was defined by the position and the relative intensity of the different rays. The crystallinity ratio (X_c) was obtained from the area of crystalline X-ray diffraction peaks after subtracting the contribution of the amorphous phase. The reciprocal of the half-height of the diffraction peak ($1/H$) located at about 19 degrees (2θ) is chosen as a reliable parameter to evaluate both size and perfection degree of crystallites; i.e., $1/H$ increases with increasing size and/or the degree of perfection.

Density

The density of the as-received and annealed samples was evaluated by using a high-precision top-loading electronic Mettler balance. The density was determined by immersing the sample in liquid ethanol.

The density of the sample was determined by the following relationship:

$$d = \frac{M_1 \cdot d_{\text{eth}} - M_2 \cdot d_{\text{air}}}{M_1 - M_2}$$

where M_1 is the weight of the PEEK sample in air; M_2 is the measured weight of PEEK sample immersed in ethanol; and d_{eth} and d_{air} are the den-

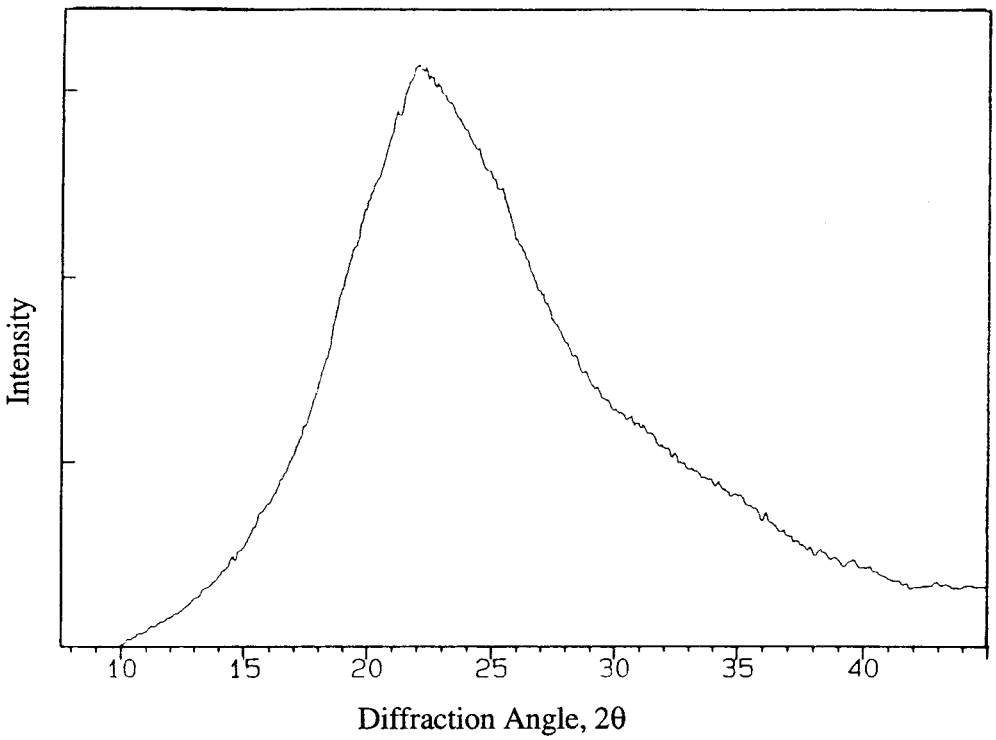

Figure 1 Wide-angle diffraction profile of the amorphous PEEK film.

sity of ethanol and air at room temperature, respectively.

Volume crystallinity fraction is determined from:

$$X_c = \frac{d - d_a}{d_c - d_a}$$

where d_c and d_a are the density of 100 and 0% crystalline PEEK, respectively. d_a, determined for as received amorphous films, is 1.263 g/cm^3, in agreement with data reported in the literature,[1,15] and d_c is chosen[25] to be 1.4 g/cm^3.

Table I Nomenclature and Annealing Conditions

Sample	Annealing Conditions
Q	Dry and freshly quenched sample
A160	Sample Q + annealing for 30 min at 160°C, then quenched
A200	Sample Q + annealing for one hour at 200°C, then quenched
A250	Sample A200 + annealing for one hour at 250°C, then quenched
A300	Sample A200 + annealing for one hour at 300°C, then quenched
A320	Sample Q + annealing for 30 min at 320°C, then quenched

Differential Scanning Calorimetry

DSC experiments were carried out from +100 to +400°C using a Perkin Elmer DSC-7 instrument for a heating rate of 100°C/min under nitrogen atmosphere. DSC traces were recorded at such an heating rate in order to limit a possible structural reorganization on heating.[13,17] Thermograms were calibrated by scanning melting-point substances, i.e., indium and zinc, at the same heating rate. This allowed two corrections to the ordinate, both of which are essential for detailed comparisons to be made. One of these is the correction for thermal lag in the differential control loop obtained from the leading edge slope of indium and zinc endotherms. The other is for thermal lag in the average control loop, which adds directly to any error in the calibration. Baselines were determined by running an empty can at the same rate of the analyzed samples, giving a curve that was subtracted from the specimen thermograms.

Dynamic Mechanical Spectrometry

Dynamic mechanical experiments were performed in tensile mode on (10×5) mm^2 sheets

Table II Characteristics of Samples Issued from WAXS Analysis and Density Measurements

Sample	X_{cm} (%)[a]	$(1/H)_{110}$[b]	d (g/cm^{-3})	X_c (%)[c]
Q	0	—	1.263	0
A160	17	1.00	1.284	16
A200	24	1.15	1.294	23
A250	28	1.25	1.299	27
A300	32	1.41	1.305	31
A320	33	1.49	1.311	35

[a] Weight crystallinity ratio determined from WAXS diffractograms.
[b] $(1/H)$ is the index of the degree of order of samples determined from the reciprocal half height of the (110) reflection profile.
[c] Volume crystallinity ratio evaluated from density measurements.

of PEEK films by using a Polymer Laboratories Mechanical Tensile Analyzer over the temperature range from −150 to +300°C for several frequencies under dry nitrogen atmosphere. This setup provides the real (E') and imaginary (E'') parts of dynamic tensile modulus and tan δ ($=E''/E'$) as functions of temperature or frequency.

For temperature scans (isochronal conditions), runs were performed in this temperature range at 1°C/min and at three frequencies, 1, 5, and 10 Hz.

Frequency scans were carried out in isothermal conditions in the same temperature range for seven frequencies ranging from 1 to 30 Hz.

RESULTS AND DISCUSSION

Density measurements, WAXS, and DSC Analysis

Volume crystallinity fraction determined from density measurements progressively increases with higher annealing temperature (Table II).

Figure 2 shows the X-ray diffractograms recorded for the annealed samples.

For each sample, the four reflection profiles characteristic of the orthorhombic phase can be observed. With increasing annealing temperature, weight crystallinity ratio increases. Moreover, the reciprocal of the half height of the diffraction peak ($1/H$) located at about 22 degrees (2θ) increases with increasing the annealing temperature. This indicates an increase in size and/or perfection degree of crystallites (Table II).

Figure 3 shows the thermograms recorded at 100°C/min for the as-received film and the annealed specimens.

The as-received sample exhibits a change in the baseline located at about 150°C, which is related to the glass transition. It is followed by a well-defined exotherm peak at about 190°C attributed to the crystallization of the amorphous sample during the heating scan. Then, crystalline phase previously formed melts at about 334°C, giving rise to an endotherm peak.

For samples annealed at 160, 200, 250, and 300°C, two melting peaks can be distinguished. The lower temperature endotherm is shifted from 175 to 315°C with an increase in the annealing temperature from 160 to 300°C. The higher temperature endotherm is at 334°C for all samples. The PEEK film annealed at 320°C only displays one endothermic peak at 334°C. According to a previous article,[17] this double melting behavior exhibited by some annealed PEEK specimens is attributed to a bimodal distribution in size and/or perfection degree of crystalline lamellae.

Moreover, for all samples, a jump in the specific heat related to the glass transition can be observed in the 140 to 150°C temperature range. With increasing annealing temperature from 20 (quenched sample) to 250°C, T_g of semicrystalline PEEK is first shifted towards the higher temperatures. Then, with an increase in the annealing temperature from 250 to 320°C, T_g is located at lower temperatures (Table III) but remains higher than T_g of the amorphous sample. The values of the specific heat jump (ΔCp) related to T_g and determined by weight unit of amorphous phase tend to increase with an increase in the annealing temperature from 200 to 320°C (Table III). Then, this could suggest that the crystallinity ratio is not the only parameter governing the molecular mobility of chains in the amorphous phase at T_g. Thus, we can recall that only the sample annealed at 320°C shows a single crystallite population, while the other semicrystalline specimens exhibit a bimodal distribution size of lamellae. Then, changes in the characteristics of T_g observed for semicrystalline films having un-

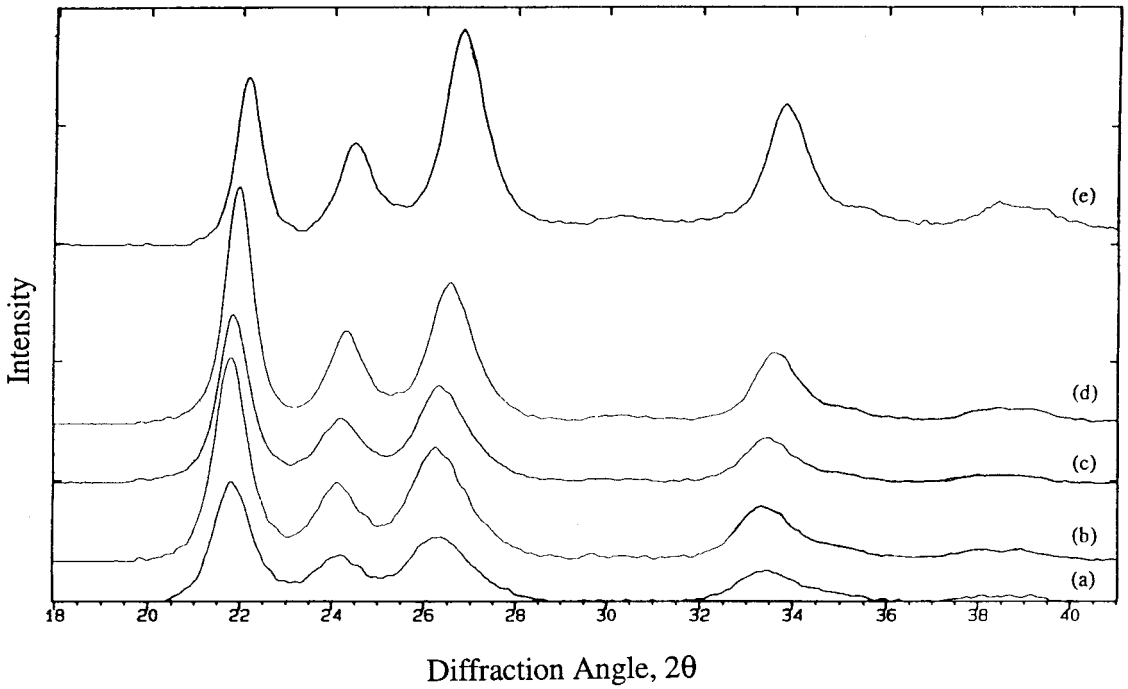

Figure 2 X-ray diffractograms of semicrystalline samples: (a) A160, (b) A200, (c) A250, (d) A300, and (e) A320.

dergone different thermal histories could be governed mainly by the broadness of the distribution size of crystalline entities. Thus, the presence of additional small (and less perfect) crystalline entities in samples annealed at temperatures lower than 300°C could enhance the decrease in the molecular mobility of chains in the amorphous phase. Such small crystallites can act as additional physical ties of the amorphous phase.

Dynamic Mechanical Spectrometry Experiments

An original and complementary method to those used previously to characterize the microstructure of PEEK is the dynamic mechanical spectrometry, carried out in both the glass temperature range and the subglass transition region of these polymers; but such an experimental method provides information not only on the microstructure of the amorphous phase assessed in terms of molecular motions of the macromolecular chains but also on the reinforcement effect of the amorphous phase by crystallites.

Glass Temperature Region

Figure 4 shows isochronal log E' and tan δ recorded at 1 Hz for the amorphous PEEK film and the annealed samples.

The amorphous film exhibits a well-defined relaxation at 148°C related to the glass transition of PEEK. The increase in the modulus observed for temperatures higher than 155°C accompanied to a weak maximum of tan δ is due to the crystallization of the sample occurring on heating. Such a phase transformation is related with the exothermic peak observed in Figure 3(a).

Table IV lists the characteristic values of the relaxation related to T_g for amorphous and semicrystalline samples. To a first approximation, the magnitude of the α relaxation of semicrystalline samples is evaluated per gram of amorphous phase to account for the presence of the crystalline phase. With respect to the α spectrum displayed by the amorphous sample, the changes in the main relaxation induced by the presence of a crystalline phase are as follows: 1) a shift of the α relaxation towards the higher temperatures, and 2) a strong decrease in the maximum of tan δ accompanied by a reducing in the magnitude of the relaxation. Such data are in agreement with conclusions from other works.[18–21]

However, it can be noted that the samples annealed at 200 and 250°C both show the strongest shift of the main relaxation towards the higher temperatures. Such variations in the location of the tan δ maximum are consistent with DSC data.

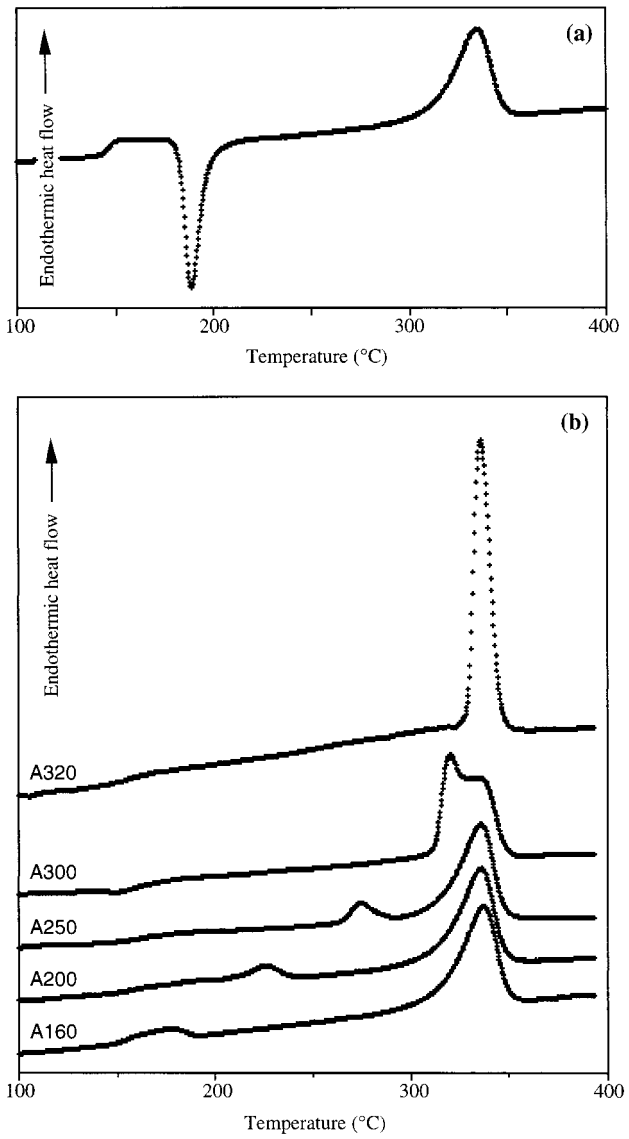

Figure 3 DSC traces recorded at 100°C/min for (a) amorphous and (b) annealed PEEK samples.

Moreover, compared with the other semicrystalline films, the sample annealed at 320°C exhibits the lowest tan δ peak temperature and the highest magnitude of the α relaxation evaluated per gram of amorphous phase. Then, it can be concluded that the thermal history, i.e., the broadness of the distribution of crystallite size, governs the molecular mobility of chains in the amorphous phase. Such an interpretation is consistent with conclusions resulting from DSC analysis.

To quantify the magnitude of interactions between phases for semicrystalline samples, it is of interest to apply a physical modeling previously developed to describe the deformation of amorphous polymers near T_g.[26]

However, before applying this modeling to the main relaxation of PEEK, it is valuable to separate the dynamic mechanical behaviors of the crystalline and the amorphous phases. The aim of such a separation in such composite materials by a mechanical model is to remove the reinforcement effect of the amorphous phase by the crystalline phase. This makes it possible to keep only the physical cross-linking effect of the amorphous phase by the crystalline entities. Among the various mechanical modelings, we have chosen the quasi-isotropic model developed by Halpin and Kardos.[27–29] Such a model, extended to describe the viscoelastic behavior according to Dickie's principle,[30] has been successfully applied to predict the mechanical behavior of polyethylene and polypropylene.[31]

The separation of the phase mechanical properties, and then the determination of the complex Young's modulus E_m^* of the amorphous phase within the semicrystalline polymer, can be performed. Detailed calculation is given in the Appendix. It requires the knowledge of the following parameters:

1. the complex Young's modulus of the semicrystalline polymer experimentally measured;
2. the values of the mechanical characteristics of the crystalline phase given by the literature[32,33];
3. the values of the volume crystallinity ratio determined from density measurements; and
4. the geometrical characteristics of the crystalline entities.

For modeling, the length of lamellae L, evalu-

Table III Characteristic Values Issued from DSC Analysis

Sample[a]	T_g (°C)	ΔC_p (J/g/K)
Q	146	0.25
A200	156	0.13
A250	156	0.13
A300	152	0.14
A320	150	0.15

[a] Characteristics of A160 are not reported here because the lower melting endotherm is very close to the glass temperature.
[b] The jump in the specific heat is determined per gram of amorphous phase.

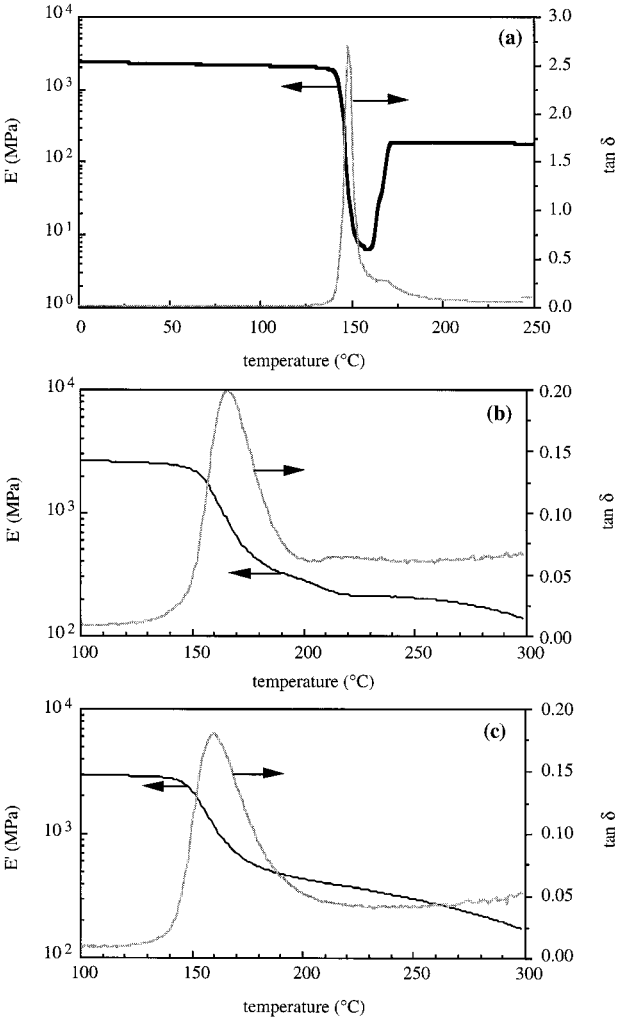

Figure 4 Dynamic mechanical behavior at 1 Hz in the α temperature range for the (a) Q, (b) A200, and (c) A320 samples.

ated by scanning electron microscopy, is about 2500 Å. The width l is estimated to be $L/10$. The average thickness has been evaluated from the melting endothermic through the Gibbs–Thomson equation.[34,35]

For example, Figure 5 shows plots of $\log E'$ and $\tan \delta$ versus temperature at 1 Hz displayed by the amorphous phase so-separated from the semicrystalline sample A300. Spectra recorded in the same conditions for the as-received amorphous and corresponding semicrystalline PEEK films are superimposed for comparison. We can note that the relaxation related to T_g of the separated amorphous phase is located at a higher temperature than that of displayed by the as-received amorphous sample, and its magnitude is significantly decreased. To a qualitative point of view, this illustrates the strong physical crosslinking effect of the amorphous phase induced by crystallites.

Table V lists characteristic values of isochronal spectra of the so-separated amorphous phase for all semicrystalline polymers.

In spite of the removal of the reinforcement effect induced by the crystalline phase, the magnitude of the main relaxation of the so-separated amorphous phase for all polymers remains significantly lower than that of the as-received amorphous PEEK film. Moreover, we can remark that the highest magnitude of the main relaxation is exhibited by the separated amorphous phase of the sample annealed at 320°C, which exhibits only a single population of crystallites. Then it can be concluded that the magnitude of the physical crosslinking effect of the amorphous phase is governed by the broadness of the crystallite size distribution, in which small crystallites act as physical ties of the amorphous phase. Such a conclusion is consistent with data issue from DSC analysis.

To quantify the magnitude of the interactions between phases, it is of interest to analyze now the isothermal mechanical behavior of the so-separated amorphous phase. Figure 6 shows the Cole–Cole diagrams of the amorphous phases of semicrystalline samples after removing the reinforcement effect brought by the crystalline phase. According to a molecular model of deformation of amorphous polymers previously developed, the complex Young's modulus E^* of the separated amorphous phase can be expressed by the following analytical expression, in which all parameters have a physical meaning[26]:

$$E^* = E_r + \frac{E_u - E_r}{1 + H(iw\tau)^{-h} + (iw\tau)^{-k}}$$

where E_u and E_r are the unrelaxed and the re-

Table IV Characteristic Parameters of the α Relaxation of PEEK Films

Samples	$T_{\alpha\max}$ (°C) at 1 Hz	Tan $\delta_{\max}$ at 1 Hz	α Peak Area (ua)[a]
Q	148	2.70	1.00
A200	166	0.20	0.54
A250	167	0.18	0.51
A300	163	0.17	0.51
A320	159	0.18	0.64

[a] The α peak area are determined per gram of amorphous phase.

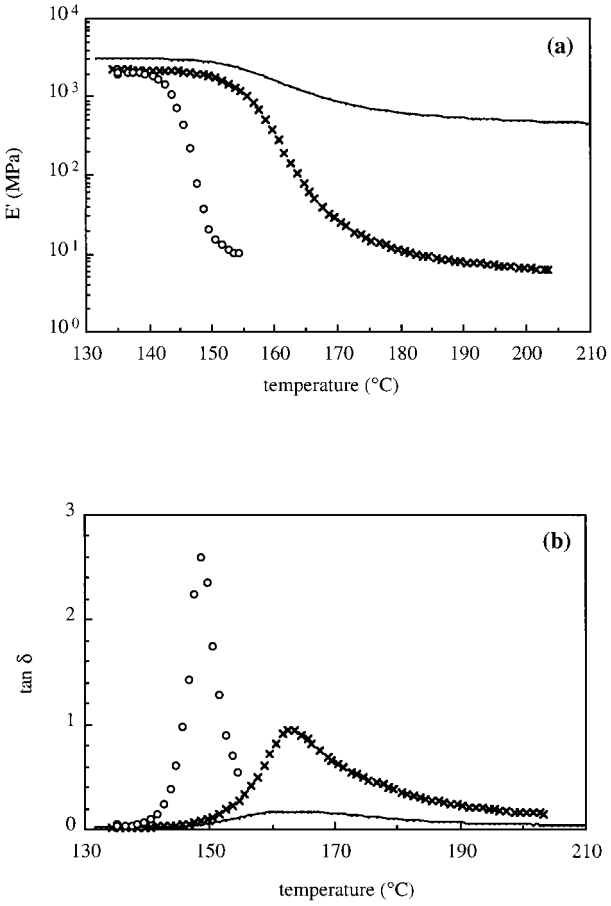

Figure 5 Plots of (a) log E' and (b) tan δ versus temperature at 1 Hz for the amorphous sample (○), the A300 semicrystalline specimen (——), and the separated amorphous phase of the A300 sample (×).

laxed moduli, and τ is the mechanical relaxation time. H is a parameter function of E_u, k, and h. k and h parameters are the correlation parameters. The k parameter decreases with decreasing the specific volume of the amorphous phase. The h parameter is very sensitive to hindrances to the molecular motions of chains. The presence of junction points, i.e., physical crosslinking ties as crystallites, hindering the deformation, leads to a decrease in the h value.

Theoretical curves issue from the physical modeling are shown in continuous line in Figure 6. Table VI lists the characteristic parameters of the separated amorphous phase for each sample. It is found that values of k and h parameters determined for the amorphous as-received PEEK film are very close to those determined for other amorphous polymers.[26,36] The unrelaxed moduli of the separated amorphous phase in semicrystalline PEEK samples are not very different from that of the as-received PEEK film. In contrast, the value of the k parameter for the amorphous phase in semicrystalline polymer tends to be lower than that of the as-received film. This could result from a decrease in the specific volume of the amorphous phase due to the presence of tie molecules. The h value is strongly decreased for amorphous phase in semicrystalline samples with respect to that of determined for the as-received amorphous sample. This is related to an increase in the magnitude of the correlation effects of molecular motions brought by the crystalline phase. This physical crosslinking effect of the amorphous phase is enhanced for samples showing the broader crystallite size distribution. To show the self-consistency of our results, it can be verified that the increase in the correlation effects observed for the amorphous phase in semicrystalline polymer is accompanied by an increase in the height of the rubbery modulus. Such a result is consistent with the qualitative interpretation issue from isochronal spectra and DSC data.

Table V Characteristic Parameters of the α Relaxation of the Separated Amorphous Phase for PEEK Samples

Samples	$T_{\alpha max}$ (°C) at 1 Hz	Tan δ_{max} at 1 Hz	α Peak Area (ua)
Q	148	2.70	1.00
A200	165	0.94	0.90
A250	166	0.92	0.87
A300	162	0.97	0.88
A320	157	1.05	1.00

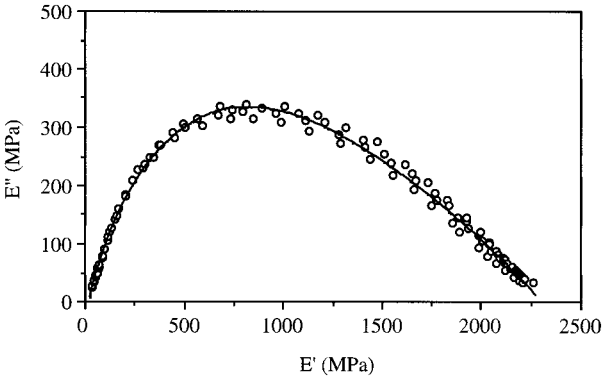

Figure 6 Experimental (○) and theoretical (full line) Cole–Cole diagrams of the separated amorphous phase of the A300 sample.

Table VI Characteristic Parameter Values of the Separated Amorphous Phase Issued from the Physical Modeling

Sample	E_u (MPa)	E_r (MPa)	k	h
Q	2200	10	0.30	0.90
A200	1900	—[a]	0.25	—[a]
A250	2100	20	0.24	0.67
A300	2300	19	0.25	0.67
A320	2100	16	0.27	0.72

[a] Characteristics of A200 at very low frequency are not reported because the lower melting temperature occurred at the end of the α relaxation.

Subglass Temperature Range (β Temperature Range)

It is also of interest to distinguish the respective contribution of the reinforcement effect from that of eventual changes in the local molecular motions induced by the crystalline phase.

In agreement with other authors,[19] we have shown in a previous article[24] that the broad β spectrum of amorphous PEEK originates from two molecular processes; i.e., the β_1 transition located at about −80°C arising from simple and noncooperative motions of the macromolecular chains, and the β_2 process located at a higher temperature and due to cooperative motions with a high activation entropy.

Tan δ spectra recorded at 1 Hz for annealed samples are shown in Figure 7, where they are compared to the spectrum of dry amorphous PEEK. With an increase in the annealing temperature, the tan δ level in the β region progressively decreases; but no shift in temperature of the maximum of the β relaxation is observed for semicrystalline polymers. Then, this could indicate that such modifications of the β spectrum of semicrystalline polymer originate mainly from mechanical coupling between phases. To give evidence for such a reinforcement effect of the amorphous phase by the crystalline entities and then to show eventual changes in the molecular motions giving rise to the β spectrum, it is valuable to compare experimental spectra to those predicted by the mechanical model, i.e., the Halpin–Kardos model. The values of the parameters used for such a modeling are the same as those used to separate the mechanical behavior of the phases near T_g.

Figure 8 shows the predicted tan δ spectra for the semicrystalline polymers.

For all semicrystalline PEEK films, the significant decrease in the β_1 relaxation height is described well by the theoretical spectrum. Then, the superimposition of the predicted and experimental data at temperatures lower than −80°C proves that the decrease in tan δ level is only due to a mechanical coupling effect between phases. It can be concluded that the presence of a crystalline phase does not induce changes in the simple molecular motion of moieties, giving rise to such a relaxation.

In contrast, the mechanical modeling predicts

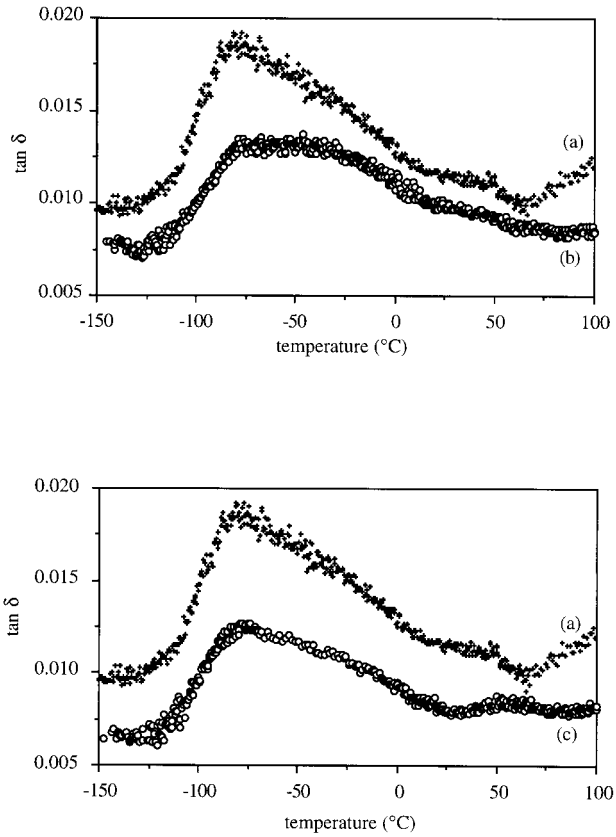

Figure 7 Plots of tan δ versus temperature at 1 Hz in the β temperature range for (a) Q, (b) A200, and (c) A320 samples.

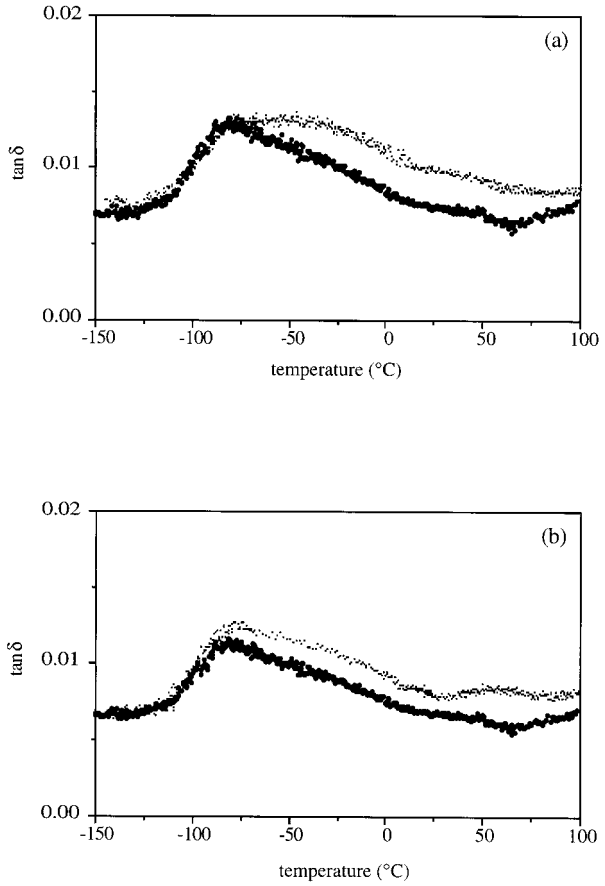

Figure 8 Plots of tan δ versus temperature at 1 Hz for (a) A200 and (b) A320 samples: experimental curve (· · · · · ·) and predicted data (•••••).

a strength of the β_2 relaxation lower than that of experimentally shown by the semicrystalline polymers. Moreover, the strength of the β_2 relaxation seems to be higher for annealed samples showing broad crystallite size distribution. Accordingly, changes in the β_2 spectrum at temperatures higher than −80°C observed for the samples annealed at 200 and 250°C could result from modifications of the molecular mobility of groups implied in this transition. Such microstructural modifications occurring in the amorphous phase could affect the conformation of the macromolecular chains near the crystalline entities and/or the magnitude of interactions between chains. Such an interpretation is consistent with data reported by other authors.[18,19,22,23]

CONCLUSIONS

The influence of a crystalline phase on the dynamic mechanical behavior of PEEK films has been analyzed over a wide range of temperatures and frequencies. Original amorphous PEEK films have undergone various annealing treatments, and then semicrystalline samples differ not only from their crystallinity ratio but also from the distribution of the crystalline phase. According to data issued from both mechanical and physical modelings, the following conclusions can be proposed.

1. The decrease in the strength of the β_1 relaxation exhibited by the semicrystalline samples with respect to the amorphous one results mainly from the mechanical coupling between phases.
2. In addition to such a reinforcement effect, the crystalline phase induces changes in the pattern of the β_2 transition, which could originate from modifications of the molecular mobility of macromolecular chains located at the vicinity of crystalline entities.
3. The strong decrease in the magnitude of the main mechanical relaxation of semicrystalline polymers results from both the reinforcement effect of the amorphous phase by crystallites and the decrease of the molecular motion ability of the chains in the amorphous phase. The physical model of the dynamic mechanical behavior of the amorphous phase gives evidence for an improvement in the magnitude of the correlation effects induced by broad crystallite size distributions.

APPENDIX

According to Halpin–Kardos modeling,[27–29] semicrystalline polymers can be treated as laminated composites, i.e., constituted of layers of oriented plies in which the ply properties are specified by the volumetric and geometric properties of each phase. Each ply is defined as a composite material in which crystalline inclusions are oriented in a given direction. Then, the semicrystalline polymer consists of a thickness-symmetric arrangement of n plies of unidirectional material making angle of π/n with respect to each other, where n is any integer greater than 2.

Two steps in the calculation must be distinguished.

In the first step, the mechanical properties of

each ply are determined by the following Halpin–Tsaï equations.[29]

$$\frac{E_{11}^*}{E_m^*} = \frac{1 + \xi_{11}\eta_{11}X_c}{1 - \eta_{11}X_c} \quad \text{with} \quad \eta_{11} = \frac{\frac{E_{11c}}{E_m^*} - 1}{\frac{E_{11c}}{E_m^*} + \xi_{11}}$$

$$\text{and } \xi_{11} = 2 \cdot \frac{L}{e} \quad (1)$$

$$\frac{E_{22}^*}{E_m^*} = \frac{1 + \xi_{22}\eta_{22}X_c}{1 - \eta_{22}X_c} \quad \text{with} \quad \eta_{22} = \frac{\frac{E_{22c}}{E_m^*} - 1}{\frac{E_{22c}}{E_m^*} + \xi_{22}}$$

$$\text{and } \xi_{22} = 2 \cdot \frac{\varrho}{e} \quad (2)$$

$$\frac{G_{12}^*}{G_m^*} = \frac{1 + \xi_{12}\eta_{12}X_c}{1 - \eta_{12}X_c} \quad \text{with} \quad \eta_{12} = \frac{\frac{G_{12c}}{G_m^*} - 1}{\frac{G_{12c}}{G_m^*} + \xi_{12}}$$

$$\text{and } \xi_{12} = \left(\frac{\varrho}{e}\right)^{\sqrt{3}} \quad (3)$$

where E_{11c} and E_{22c} are the elastic moduli of crystalline phase in the directions 1 and 2; G_{12c} is the in-plane elastic shear modulus of the crystalline phase; E_{11}^* and E_{22}^* are the complex moduli of semicrystalline polymer in the directions 1 and 2; G_{12}^* is the in-plane complex shear modulus of the semicrystalline polymer; L, l and e, are the length, the width and the thickness of the crystalline lamellae, respectively; X_c is the volume crystallinity ratio of the polymer; E_m^* is the complex Young's modulus of the amorphous phase experimentally determined; and G_m^* is the complex shear modulus of the amorphous phase determined through the following expression.

$$G_m^* = \frac{E_m^*}{2 \cdot (1 + \nu_m)} \quad (4)$$

where ν_m is the Poisson's ratio of the amorphous phase.

In the second step, the complex shear modulus G^* of the semicrystalline polymer can be expressed through the following equation of Halpin–Kardos:

$$G^* = \frac{1}{8 \cdot (1 - \nu_{12} \cdot \nu_{21})} E_{11}^* + \frac{1 - 2\nu_{12}}{8 \cdot (1 - \nu_{12} \cdot \nu_{21})} E_{22}^* + \frac{1}{2} G_{12}^* \quad (5)$$

where ν_{12} and ν_{21} are the Poisson's ratios of semicrystalline polymer. For calculation, ν_{12} and ν_{21} are assumed to be real and equal, expressed by

$$\nu_{12} = \nu_{21} = X_c\nu_c + (1 - X_c)\nu_m \quad (6)$$

where ν_c is the Poisson's ratio of the crystalline phase.

The complex Young's modulus E_m^* of the amorphous phase within the semicrystalline polymer can be assessed through the inversion of the eq. (5), which can be also expressed as

$$G^* = \sum_{i=1}^{2} \frac{a_{ii} \cdot E_m^* + b_{ii}}{c_{ii} \cdot E_m^* + d_{ii}} \cdot E_m^* + \frac{a_{12} \cdot E_m^* + b_{12}}{c_{12} \cdot E_m^* + d_{12}} \cdot E_m^* \quad (7)$$

where a_{ij}, b_{ij}, c_{ij}, and d_{ij} are functions of ξ_{ij}, X_c, ν_m, E_{11c}, E_{22c}, and G_{12c}; and G^* is the complex shear modulus of the amorphous phase in the semicrystalline polymer.

To determine the complex Young's modulus E_m^* of the amorphous phase, we have divided such a complex equation of the fourth degree of variable E_m^* in a system of two real equations of the fourth degree of variable E_m''.

Coefficients of these two equations are functions of the real part of Young's modulus E_m'. Such a system is then converted into the two following equations:

$$\begin{cases} f(E_m') = 0 & (8) \\ E_m'' = g(E_m') & (9) \end{cases}$$

which are solved numerically.

The authors are grateful to Mr. K. D. Gilliatt and Mrs. A. Guinet (ICI film, United Kingdom and France) for providing amorphous PEEK films. They are also indebted to Pr Legras (Laboratoire des Hauts Polymères, Université Catholique de Louvain-la-Neuve, Belgium) for molecular weight measurements. They are grateful to Mrs. F. Thimon and Mrs. C. Bertrand (LSM, Annecy,

France) for their technical help in the X-ray experiments.

REFERENCES

1. D. J. Blundell and B. N. Osborn, *Polymer,* **24,** 953 (1983).
2. A. Jonas and R. Legras, *Polymer,* **32,** 2691 (1991).
3. Y. Lee and R. S. Porter, *Macromolecules,* **1,** 2770 (1988).
4. D. C. Basset, R. H. Olley, and I. A. M. Al Raheil, *Polymer,* **29,** 1745 (1988).
5. P. Cebe and S. D. Hong, *Polymer,* **27,** 1183 (1986).
6. C. M. Hsiung, M. Cakmak and J. L. White, *Polym. Eng. Sci.,* **30,** 967 (1990).
7. A. Jonas, R. Legras, and J. P. Issi, *Polymer,* **32,** 3364 (1991).
8. A. Franbourg and F. Rietsch, *Polym. Bull.,* **24,** 445 (1990).
9. M. P. Lattimer, J. K. Hoobs, M. J. Hill, and P. J. Barham, *Polymer,* **33,** 3971 (1992).
10. G. S. H. Gupta and R. Salovey, *Polym. Eng. Sci.,* **30,** 453 (1990).
11. Y. Deslandes, M. Day, N. F. Sabir, and T. Suprunchuk, *Polym. Comp.,* **10,** 360 (1989).
12. S. Kumar, P. Anderson, and W. W. Adams, *Polymer,* **27,** 329 (1986).
13. Y. Lee, R. S. Porter, and J. S. Lin, *Macromolecules,* **22,** 1756 (1989).
14. S. S. Chang, *Polym. Commun.,* **29,** 138 (1988).
15. D. J. Blundell, *Polymer,* **28,** 2248 (1987).
16. Y. Lee and R. S. Porter, *Macromolecules,* **20,** 1336 (1987).
17. C. Bas, P. Battesti, and N. D. Alberola, *J. Appl. Polym. Sci.,* **53,** 1745 (1994).
18. A. Jonas and R. Legras, *Macromolecules,* **26,** 813 (1993).
19. R. K. Krishnaswamy and D. S. Kalika, *Polymer,* **35,** 1157 (1994).
20. L. David and S. Etienne, *Macromolecules,* **26,** 4489 (1993).
21. P. Huo and P. Cebe, *Macromolecules,* **25,** 902 (1992).
22. T. Sasuga and M. Hagiwara, *Polymer,* **27,** 821 (1986).
23. D. S. Kalika and R. K. Krishnaswamy, *Macromolecules,* **26,** 4252 (1993).
24. C. Bas and N. D. Albérola, *Polym. Eng. Sci.,* **36,** 244 (1996).
25. A. Jonas, PhD Thesis, Université Catholique de Louvain, 1992.
26. J. Perez, *Physique et Mécanique des Polymères Amorphes,* Technique et Documentation, Lavoisier Ed., Paris, 1992.
27. J. C. Halpin and J. L. Kardos, *Polym. Eng. Sci.,* **16,** 344 (1976).
28. J. C. Halpin and J. L. Kardos, *J. Appl. Phys.,* **43,** 2235 (1972).
29. J. L. Kardos, J. Raisoni, S. Piccarolo, and J. C. Halpin, *Polym. Eng. Sci.,* **19,** 1000 (1979).
30. R. A. Dickie, *J. Appl. Polym. Sci.,* **17,** 45 (1973).
31. N. Albérola, J. Y. Cavaille, and J. Perez, *Eur. Polym. J.,* **28,** 949 (1992).
32. T. Nishino, K. Tada, and K. Nakamae, *Polymer,* **33,** 736 (1992).
33. A. J. Lovinger and D. D. Davis, *J. Phys. Appl.,* **58,** 2843 (1985).
34. J. I. Lauritzen and J. D. Hoffman, *J. Res. NBS,* **64A,** 73 (1960).
35. B. Wunderlich, *Macromolecular Physics,* Vol. 2, Academic Press, New York, 1980.
36. A. Bergeret, N. Albérola, A. Agbossou, P. Cassagnau, and T. Sarraf, *Eur. Polym. J.,* **28,** 1201 (1992).